Catalysis Today 158 (2010) 464–469

Contents lists available at ScienceDirect

Catalysis Today

journal homepage: www.elsevier.com/locate/cattod

Dehydrogenation of ethylbenzene to styrene with CO_2 over iron oxide-based catalysts

Min Ji[a,*], Guili Chen[a], Junhu Wang[b,**], Xinkui Wang[a], Tao Zhang[b]

[a] Department of Chemistry, School of Chemical Engineering, Dalian University of Technology, Dalian 116012, PR China
[b] State Key Laboratory of Catalysis, Dalian Institute of Chemical Physics, Chinese Academy of Sciences, Dalian 116023, PR China

ARTICLE INFO

Article history:
Available online 19 August 2010

Keywords:
Ethylbenzene
Oxidative dehydrogenation
Carbon dioxide
Iron oxide-based catalysts

ABSTRACT

This paper describes dehydrogenation reaction of ethylbenzene to styrene with CO_2 over iron oxide-based catalysts. Three catalysts of Fe_2O_3–MgO/γ-Al_2O_3, $Fe_2O_3/MgAl_2O_4$ and $MgFe_{0.1}Al_{1.9}O_4$ with the same molar ratio of Mg/Fe/Al were prepared by impregnation and sol–gel methods. At 580 °C, the ethylbenzene conversion over $MgFe_{0.1}Al_{1.9}O_4$ kept a value of 40% during the time on stream of 20 h, whereas that over $Fe_2O_3/MgAl_2O_4$ decreased rapidly from initial 50.0% to 27.4%. The properties of the catalysts were characterized by several techniques such as N_2 adsorption/desorption, X-ray diffraction, thermogravimetry, energy dispersive X-ray spectroscopy, Fourier transform-infrared spectroscopy, ^{57}Fe Mössbauer spectroscopy, temperature-programmed reduction, and temperature-programmed desorption of NH_3 and CO_2. It was found that the iron species of these catalysts are different. In $MgFe_{0.1}Al_{1.9}O_4$, all Fe^{3+} species are incorporated in the spinel lattice. $MgFe_{0.1}Al_{1.9}O_4$ shows high catalytic activity and stability in ethylbenzene dehydrogenation reaction with CO_2. Moreover, the weak surface acidity of $MgFe_{0.1}Al_{1.9}O_4$ prevents from the carbon formation during the reaction.

1. Introduction

Styrene (ST) is one of the most important raw materials for polymers production. It is commercially produced by the dehydrogenation of ethylbenzene (EB) in the presence of a large quantity of steam at high temperatures ranging from 600 to 700 °C. Due to its highly endothermic character, the superheated steam is used to supply the heat, and it is not recovered in this process [1]. In past decades, CO_2 has received much attention as a co-feed gas instead of steam since it could reduce energy required for producing ST and increase the ST yield at reaction equilibrium. The dehydrogenation of EB to ST in the presence of CO_2 is believed to be an energy-saving and environmentally friendly process [2–11]. High performance catalysts have been screened extensively, such as iron oxide-based catalysts supported on Al_2O_3 [4] and active carbon [5], vanadium oxide catalysts supported on Al_2O_3 [6], MgO [7], SBA-15 [8], and active carbon [9], catalysts obtained by thermal decomposition of hydrotalcite-like precursors [10], and ZrO_2 [11]. Among these catalysts, iron oxide-based catalysts were more effective for the ethelbenzene dehydrogenation with CO_2. However, the fast deactivation due to the coke deposition, sintering of the active species and the change in valence state of iron still restrain the practical utilization of iron oxide-based catalysts. In order to enhance its lifetime, many studies were focused on the addition of alkaline metals (Li, Na and K) or alkali earth metals (Ca and Mg) as promoters to inhibit the carbon deposition [2,12,13]. In this study, a ternary-composite oxide of iron-incorporated catalyst which exhibits high stability in EB dehydrogenation in the presence of CO_2 was reported. The relationship between the type of iron species and the catalytic performance of iron catalyst was discussed.

2. Experimental

2.1. Catalyst preparation

Three catalysts of Fe_2O_3–MgO/γ-Al_2O_3, $Fe_2O_3/MgAl_2O_4$ and $MgFe_{0.1}Al_{1.9}O_4$ were prepared with the same molar ratio of Mg/Fe/Al of 1:0.1:1.9. $MgAl_2O_4$ support and $MgFe_{0.1}Al_{1.9}O_4$ catalyst were prepared by sol–gel method. Magnesium nitrate, aluminum nitrate and iron nitrate were used as the starting materials. The solution of metal nitrates with stoichiometric ratio was added to a solution of citric acid and stirred at 80 °C until the gelation occurred, resulting gels were dried at 120 °C for 48 h, and then calcined at 700 °C for 4 h.

Fe_2O_3–MgO/γ-Al_2O_3 and $Fe_2O_3/MgAl_2O_4$ catalysts were prepared by impregnation method. γ-Al_2O_3 and $MgAl_2O_4$ synthesized

* Corresponding author. Tel.: +86 411 39893637; fax: +86 411 83631333.
** Corresponding author. Tel.: +86 411 84379159; fax: +86 411 84685940.
E-mail addresses: jimin@dlut.edu.cn (M. Ji), wangjh@dicp.ac.cn (J. Wang).

0920-5861/$ – see front matter © 2010 Elsevier B.V. All rights reserved.
doi:10.1016/j.cattod.2010.07.014

Table 1
Initial EBDH activity on the iron oxide-based catalysts.

Catalyst	X_{EB} (%)	Selectivity			ST yield (%)
		Styrene	Benzene	Toluene	
Fe_2O_3–MgO/γ-Al_2O_3	24.5	97.1	1.60	1.30	23.8
$Fe_2O_3/MgAl_2O_4$	50.0	95.7	2.17	2.13	47.9
$MgFe_{0.1}Al_{1.9}O_4$	40.9	95.3	2.09	2.61	39.0

Reaction conditions: LHSV = 1.12 h^{-1}, CO_2/EB = 5/1, time on stream = 2 h, temperature = 580 °C.
X_{EB}: EB conversion.

above were dipped into the solution of magnesium nitrate and/or iron nitrate, the excess water was slowly evaporated with stirring on a water bath, the resulting solids were dried at 120 °C, then calcined at 700 °C for 4 h. These catalysts were crushed, and sieved into granules of 20–40 mesh for the reaction of ethelbenzene dehydrogenation with CO_2.

2.2. Catalyst characterization

The BET surface areas of the catalysts were measured by nitrogen physisorption at −196 °C with a surface area analyzer, Micromeritics ASAP 2000. The samples were treated at 350 °C in vacuum for 3 h before N_2 physisorption measurements. Thermogravimetric (TG) analysis of the catalysts was performed on a TGA/SDTA 851e Mettler analyzer. The samples were heated from room temperature to 800 °C in an air flow of 80 ml/min with a heating rate of 10 °C/min. X-ray powder diffraction (XRD) experiments were carried out on a D/Max 2400 diffractometer with Cu K_α radiation (λ = 1.5418 Å). Energy dispersive X-ray spectroscopic (EDS) analysis was performed on a JSM-5600LV scanning electron microscope to measure the Mg, Fe, and Al composition on the surface of catalysts.

Fourier transform-infrared spectra (FT-IR) of the samples were recorded on Shimadzu FT-IR 460 at ambient conditions using a KBr pellet technique. The ^{57}Fe Mössbauer spectra (^{57}Fe MS) were measured by a Topologic MFD-500A Mössbauer spectrometer at room temperature, a ^{57}Co source in rhodium matrix was used. The Doppler velocity of the spectrometer was calibrated with respect to α-Fe foils. The spectra were fitted with superpositions of Lorentzian lines using the MossWinn 3.0i program. Temperature-programmed reduction (H_2-TPR) experiments were carried out in a setup equipped with a temperature programmable furnace. Each sample was pretreated at 500 °C for 30 min in high-purity (99.9%) nitrogen flow of 20 ml/min. After cooling to ambient temperature, TPR experiments were performed in 5% H_2/N_2 mixture flow at a heating rate of 10 °C/min. The amount of hydrogen consumed was monitored with a thermal conductivity detector (TCD).

To investigate the surface acidity and basicity of the catalysts, temperature-programmed desorption of NH_3 (NH_3-TPD) and CO_2 (CO_2-TPD) was performed on a Micromeritics AutoChem 2920 analyzer. The sample (∼0.1 g) was charged into a quartz reactor and treated in helium at 500 °C for 1 h, then exposed to CO_2 or NH_3 at 50 °C for 1 h, and purged by helium to remove gas phase and physically adsorbed CO_2 or NH_3. The sample was heated from 50 to 800 °C at a rate of 10 °C/min, and the amount of desorbed CO_2 or NH_3 was monitored by the means of a TCD.

2.3. Catalytic tests

Catalytic reactions were performed in a fixed-bed reactor (i.d. 8.0 mm and length 300 mm) at 580 °C under atmospheric pressure. 1.0 g of a catalyst was placed at the center of the reactor with quartz wool plugs. The molar ratio of CO_2/EB is 5. The products were analyzed by gas chromatography on Agilent-6890: aromatic compounds were analyzed by a FID detector using capillary column of HP-5, and gaseous products were analyzed by a TCD detector using a packed carbon molecular sieve column.

3. Results and discussion

3.1. Catalytic performance

The initial EB conversion, ST selectivity and ST yield over the Fe-containing catalysts are summarized in Table 1. It can be seen that the EB conversions increase in the sequence of Fe_2O_3–MgO/γ-Al_2O_3, $MgFe_{0.1}Al_{1.9}O_4$, $Fe_2O_3/MgAl_2O_4$. Fig. 1 shows the change in trend of EB conversion with reaction time on stream. It can be seen that $MgFe_{0.1}Al_{1.9}O_4$ exhibited much higher stability than that of $Fe_2O_3/MgAl_2O_4$. The EB conversion over $Fe_2O_3/MgAl_2O_4$ decreases rapidly from 50.0% to 27.4% after 20 h, whereas no evident decrease in the conversion is observed over $MgFe_{0.1}Al_{1.9}O_4$ catalyst. The results indicated that $MgFe_{0.1}Al_{1.9}O_4$ possesses optimal activity and stability among these three catalysts.

Recently, Liu et al. studied the EBDH over the catalyst of La_2O_3–V_2O_5/MCM-41, and the high EB conversion of 86.5% and styrene selectivity of 91.0% were obtained under the reaction conditions of 600 °C and CO_2/EB molar ratio of 10 [14]. Noteworthy, Park et al. reported 60% EB conversion and about 98% styrene selectivity over the catalyst of V_2O_5–CeO_2/TiO_2–ZrO_2 at 600 °C, and activity was kept for 10 h [15]. Compared with these results, the catalytic performance over $MgFe_{0.1}Al_{1.9}O_4$ is remarkable.

3.2. Catalyst characterization

3.2.1. BET and TG

The BET surface areas (S_{BET}) of the fresh and used catalysts are listed in Table 2. The S_{BET} values of Fe_2O_3–MgO/γ-Al_2O_3 and $Fe_2O_3/MgAl_2O_4$ apparently decrease after reaction from 202 to 160 m^2/g and from 112 to 70 m^2/g, respectively, whereas the surface area of $MgFe_{0.1}Al_{1.9}O_4$ has no change after the 20-h reaction. It implies that $MgFe_{0.1}Al_{1.9}O_4$ is an anti-sintering catalyst. The amount of carbon deposition after the reaction measured by TG technique was shown in Table 2. The least weight loss of

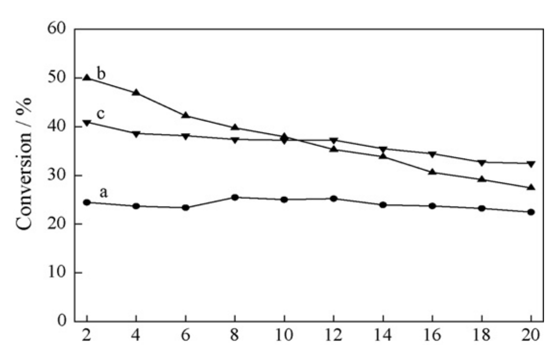

Fig. 1. BE conversion as a function of time on stream over catalysts: (a) Fe_2O_3–MgO/γ-Al_2O_3, (b) $Fe_2O_3/MgAl_2O_4$, and (c) $MgFe_{0.1}Al_{1.9}O_4$.

Table 2
BET surface areas and the weight loss of used catalysts.

Catalyst	S_{BET} (m^2/g)		Weight loss (%)
	Fresh	Used	
Fe_2O_3–MgO/γ-Al_2O_3	202	160	27.2
$Fe_2O_3/MgAl_2O_4$	112	70	21.3
$MgFe_{0.1}Al_{1.9}O_4$	106	109	12.4

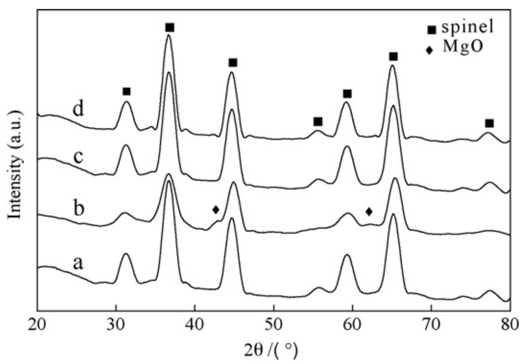

Fig. 2. X-ray diffraction patterns for $MgAl_2O_4$ support and catalysts: (a) $MgAl_2O_4$, (b) Fe_2O_3–MgO/γ-Al_2O_3, (c) $Fe_2O_3/MgAl_2O_4$, and (d) $MgFe_{0.1}Al_{1.9}O_4$.

$MgFe_{0.1}Al_{1.9}O_4$ means the weakest carbon deposition among these three catalysts. So, the good activity and stability of $MgFe_{0.1}Al_{1.9}O_4$ is in agreement with its strong resistance capacities to carbon deposition and sintering.

3.2.2. XRD and EDS

The XRD patterns of $MgAl_2O_4$ support and three iron oxide-based catalysts were displayed in Fig. 2. For all three catalysts, there are no diffraction peaks of α-Fe_2O_3, but small diffraction peaks of MgO in Fe_2O_3–MgO/γ-Al_2O_3. Comparing with $MgAl_2O_4$, all the diffraction peaks of iron-containing catalysts shifted forward to small angle, which is caused by the unit cell expansion. The data of cell parameters listed in Table 3 verified the unit cell expansion, which could be caused by iron substitution for Al^{3+} and/or Mg^{2+} in the $MgAl_2O_4$ spinel lattice since the radius of Fe^{3+} (0.064 nm) and Fe^{2+} (0.074 nm) are bigger than that of Al^{3+} (0.050 nm) and Mg^{2+} (0.065 nm), respectively. The bigger lattice constant of $MgFe_{0.1}Al_{1.9}O_4$ implies that the amount of Fe incorporated into spinel lattice is more. For catalyst of Fe_2O_3–MgO/γ-Al_2O_3, the big lattice constant is also related to its low crystallinity of only 71.93%, which is similar with that in the literature [16].

In order to characterize the content of Fe species dispersed in catalyst surface, the surface composition was determined by EDS, and the results were shown in Table 4. Nearly the same Mg contents are observed on three catalysts surfaces, whereas the ratio of Fe/Al decreases from Fe_2O_3–MgO/γ-Al_2O_3, $Fe_2O_3/MgAl_2O_4$ to $MgFe_{0.1}Al_{1.9}O_4$. For catalyst $MgFe_{0.1}Al_{1.9}O_4$, the surface molar ratio of Mg:Fe:Al (1:0.075:1.87) is very close to its stoichiometric ratio of 1:0.1:1.9. On the other hand, the Fe contents on the surface of Fe_2O_3–MgO/γ-Al_2O_3 and $Fe_2O_3/MgAl_2O_4$ are much higher than its stoichiometric ratio. These results suggest that iron species partially enriched on the surface of both Fe_2O_3–MgO/γ-Al_2O_3 and $Fe_2O_3/MgAl_2O_4$ catalysts. In the case of $MgFe_{0.1}Al_{1.9}O_4$, iron species are incorporated uniformly in the spinel lattice.

Table 3
Lattice constant and crystallinity of the catalysts.

Catalyst	Lattice constant (Å)	Crystallinity (%)
Fe_2O_3–MgO/γ-Al_2O_3	8.1883	71.93
$Fe_2O_3/MgAl_2O_4$	8.0906	82.60
$MgFe_{0.1}Al_{1.9}O_4$	8.1163	84.27

Table 4
Distribution of atoms in catalyst surface.

Catalyst	Atomic (%)			Atomic ratio Mg:Fe:Al
	Mg	Fe	Al	
Fe_2O_3–MgO/γ-Al_2O_3	36.40	15.33	48.27	1:0.42:1.33
$Fe_2O_3/MgAl_2O_4$	36.20	6.10	57.70	1:0.17:1.59
$MgFe_{0.1}Al_{1.9}O_4$	34.00	2.55	63.45	1:0.075:1.87

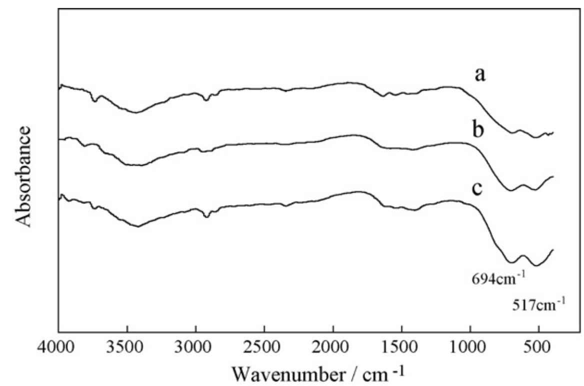

Fig. 3. FT-IR spectra of catalysts: (a) Fe_2O_3–MgO/γ-Al_2O_3, (b) $Fe_2O_3/MgAl_2O_4$, and (c) $MgFe_{0.1}Al_{1.9}O_4$.

3.2.3. FT-IR

Fig. 3 shows the FT-IR spectra of catalysts. Two bands peaked at ∼694 and ∼517 cm^{-1} indicate the formation of $MgAl_2O_4$ spinel [17]. The high frequency band at 694 cm^{-1} is due to bond between octahedral cation and oxygen anion, and the low frequency band at 517 cm^{-1}corresponds to the complex vibration involved octahedral and tetrahedral cations [18]. In Fig. 3 it can be found that absorbance peaks became sharper following the catalyst order from Fe_2O_3–MgO/γ-Al_2O_3, $Fe_2O_3/MgAl_2O_4$ to $MgFe_{0.1}Al_{1.9}O_4$, indicating the crystallinity increase of spinel phase in the catalysts, which is in agreement with XRD results.

3.2.4. H_2-TPR

The TPR profiles of the catalysts in Fig. 4 show very different reduction behaviors of the catalysts. There are three reduction peaks at 456, 516 and 651 °C in the TPR profile of Fe_2O_3–MgO/γ-Al_2O_3 (Fig. 4a). According to literatures [19,20], the peak at 456 °C is assigned to the reduction process of $Fe^{3+} \rightarrow Fe^{2+}$ of α-Fe_2O_3, and the second peak at 516 °C is ascribed to the reduction of Fe^{3+} in

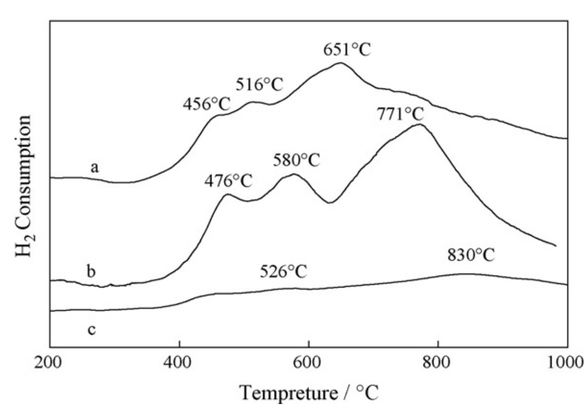

Fig. 4. H_2-TPR profiles of catalysts: (a) Fe_2O_3–MgO/γ-Al_2O_3, (b) $Fe_2O_3/MgAl_2O_4$, and (c) $MgFe_{0.1}Al_{1.9}O_4$.

Table 5
^{57}Fe Mössbauer parameters of the catalysts before and after the catalytic reaction.

Catalyst	IS (mm/s)	QS (mm/s)	*H* (T)	LW (mm/s)	Area (%)	Remarks
Fe_2O_3–MgO/γ-Al_2O_3 fresh	0.59	1.64		0.58	4.4	Fe^{2+} in Td
	0.27	0.81		0.58	68.1	Fe^{3+}in Oh
	0.35	−0.22	50.2	0.43	27.5	α-Fe_2O_3(m)
Fe_2O_3–MgO/γ-Al_2O_3 used	0.59	1.64		0.71	16.2	Fe^{2+} in Td
	0.33	0.70		0.58	59.1	Fe^{3+} in Oh
	0.36	−0.11	46.3	0.58	9.8	Fe_3O_4
	0.71	2.12		0.58	14.9	$Fe^{3+} \to Fe^{2+}$
$Fe_2O_3/MgAl_2O_4$ fresh	0.25	0.80		0.58	80.3	Fe^{3+} in Oh
	0.37	1.03		0.58	19.7	α-Fe_2O_3(s)
$Fe_2O_3/MgAl_2O_4$ used	0.25	0.82		0.58	58.9	Fe^{3+} in Oh
	0.53	0.98		0.58	27.3	$Mg_xFe_{1-x}O$
	0.64	2.29		0.58	13.9	$Fe^{3+} \to Fe^{2+}$
$MgFe_{0.1}Al_{1.9}O_4$ fresh	0.59	1.64		0.58	8.5	Fe^{2+} in Td
	0.27	0.86		0.58	91.5	Fe^{3+} in Oh
$MgFe_{0.1}Al_{1.9}O_4$ used	0.59	1.64		0.58	12.7	Fe^{2+} in Td
	0.29	0.80		0.58	76.1	Fe^{3+} in Oh
	0.70	2.43		0.51	11.1	$Fe^{3+} \to Fe^{2+}$

IS: isomer shift; QS: electric quadrupole splitting; *H*: magnetic field; LW: full linewidth at half maximum; area: relative resonance areas of the different components of the absorption patterns.

$MgAl_2O_4$ lattice to Fe^{2+}. The peak at 651 °C is related to the further reduction of Fe^{2+} to metallic Fe. From Fig. 4 it can be seen that the reduction profile of $Fe_2O_3/MgAl_2O_4$ (Fig. 4b) is approximately the same as that of Fe_2O_3–MgO/γ-Al_2O_3 except the reduction peaks shifted to higher temperature, which might be caused by the strong interaction between Fe_2O_3 and $MgAl_2O_4$. Since the catalyst of Fe_2O_3–MgO/γ-Al_2O_3 was prepared by the co-impregnation of iron nitrate and magnesium nitrate solution, the lower reduction temperature of its iron species indicates that the addition of magnesium in the preparation process can decrease the interaction of iron with γ-Al_2O_3 support. The TPR profile of $MgFe_{0.1}Al_{1.9}O_4$ reveals only two low reduction bands peaked at ∼520 °C and ∼830 °C, which could be ascribed to the sequential reduction process of $Fe^{3+} \to Fe^{2+} \to Fe^0$ in spinel.

3.2.5. ^{57}Fe MS

^{57}Fe Mössbauer spectroscopy is a powerful technique to identify the coordination environment and valence state of iron. ^{57}Fe Mössbauer spectra of the fresh and used catalysts were measured at room temperature, as shown in Fig. 5. The data of all ^{57}Fe Mössbauer spectra are listed in Table 5.

For fresh Fe_2O_3–MgO/γ-Al_2O_3, the ^{57}Fe Mössbauer spectra are fitted with a sextuplet and two doublet peaks. The sextuplet peak with an isomer shift of 0.35 is characteristic of α-Fe_2O_3 with large particle size, which possesses very low dispersion and very weak relationship with the support [19]. One doublet with the isomer shift of 0.59 mm/s is assigned to Fe^{2+} in the tetrahedral site of spinel, and another doublet with the isomer shift of 0.27 mm/s is due to Fe^{3+} in octahedral [20]. This result noted that the iron species of Fe_2O_3–MgO/γ-Al_2O_3 incorporated not only in tetrahedral site but also in octahedral site of the spinel, and 68.1% of iron species is located in octahedral site. The presence of Fe^{2+} and Fe^{3+} in spinel lattice indicates that the Mg–Fe–Al–O mixed oxide formed in Fe_2O_3–MgO/γ-Al_2O_3 catalyst. After the reaction, the relative contents of Fe^{2+} and Fe^{3+} in the spinel of Fe_2O_3–MgO/γ-Al_2O_3 are changed, with the increase of Fe^{2+} and decrease of Fe^{3+}. In addition, two new spectra appeared. The sextuplet with isomer shift of 0.36 is assigned to Fe_3O_4, which results from the partially reduction of α-Fe_2O_3, the species with isomer shift of 0.71 mm/s is attributed to Fe^{2+} in $FeAl_2O_4$ formed in the interfaces between α-Fe_2O_3 and γ-Al_2O_3 during the reaction [21].

The Mössbauer spectra of the fresh $Fe_2O_3/MgAl_2O_4$ catalyst are fitted with two doublets. One with isomer shift of 0.25 mm/s is assigned to Fe^{3+} in octahedral site of $MgAl_2O_4$ spinel, and the other one with isomer shift of 0.37 mm/s is attributed to highly dispersed α-Fe_2O_3 particles [22]. After reaction, the α-Fe_2O_3 disappeared, and two new doublets are observed, one with isomer shift of 0.53 mm/s is assigned to $Mg_{1-x}Fe_xO$ as reported previously by several groups [19,23–25], which means that a part of $MgAl_2O_4$ support might decompose in the EBDH reaction process, and Mg–Fe–O forms. The other characterized with isomer shift of 0.64 mm/s is assigned to Fe^{2+}, which is the same species with that of the newly appeared in the used Fe_2O_3–MgO/γ-Al_2O_3 catalyst.

The Mössbauer spectra of fresh $MgFe_{0.1}Al_{1.9}O_4$ are fitted with two doublets, corresponding to the tetrahedral Fe^{2+} and the octahedral Fe^{3+} in spinel, respectively. Both of them are still observed in used $MgFe_{0.1}Al_{1.9}O_4$, although their relative contents have been changed. After the reaction, the content of the octahedral Fe^{3+} decreases, and that of tetrahedral Fe^{2+} increases, indicating that partial Fe^{3+} was reduced during the reaction. The new doublet with isomer shift of 0.70 mm/s is also attributed to Fe^{2+} in $FeAl_2O_4$ as above.

From the ^{57}Fe Mössbauer results of three catalysts before and after EBDH reaction, it can be seen that the decrease of Fe^{3+} species due to the reduction, the increase of Fe^{2+}, and the formation of $FeAl_2O_4$ during the reaction. $FeAl_2O_4$ phase prevents from the further reduction of Fe^{2+}, and the formation of iron carbide during the reaction [26]. The disappearance of small particle α-Fe_2O_3 during the reaction in catalyst $Fe_2O_3/MgAl_2O_4$ may be responsible for its rapid deactivation.

Above-mentioned characterization of XRD, EDS, ^{57}Fe Mössbauer and H_2-TPR indicated that the preparation method greatly influences the state of iron species in the catalysts. By sol–gel method, Fe^{3+} ion species proportionately incorporated into the spinel lattice to form $MgFe_{0.1}Al_{1.9}O_4$ catalyst, whereas by the impregnation method, Fe^{3+} ion species forms partially α-Fe_2O_3 dispersed on catalyst surface. The highly dispersed α-Fe_2O_3 was detected in $Fe_2O_3/MgAl_2O_4$, and the α-Fe_2O_3 with relatively large particle size formed in Fe_2O_3–MgO/γ-Al_2O_3 catalyst.

3.2.6. TPD

The CO_2-TPD profiles of the catalysts are shown in Fig. 6. It can be seen that both of $Fe_2O_3/MgAl_2O_4$ and $MgFe_{0.1}Al_{1.9}O_4$ exhibits

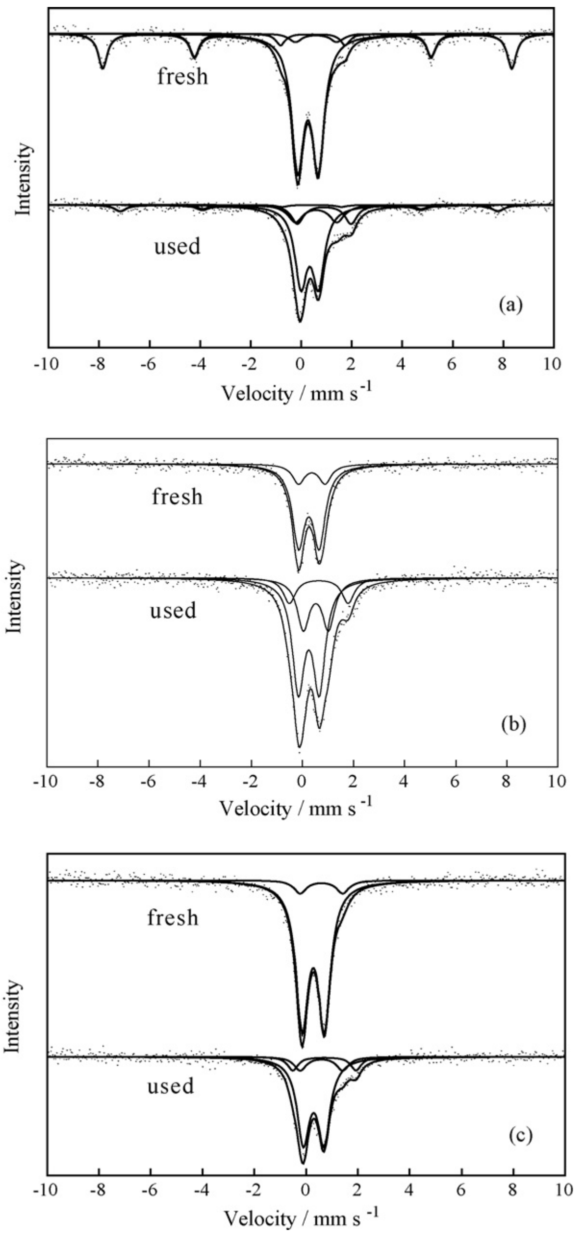

Fig. 5. ^{57}Fe Mössbauer spectra of catalysts before and after reaction (a) Fe_2O_3–MgO/γ-Al_2O_3, (b) $Fe_2O_3/MgAl_2O_4$, and (c) $MgFe_{0.1}Al_{1.9}O_4$.

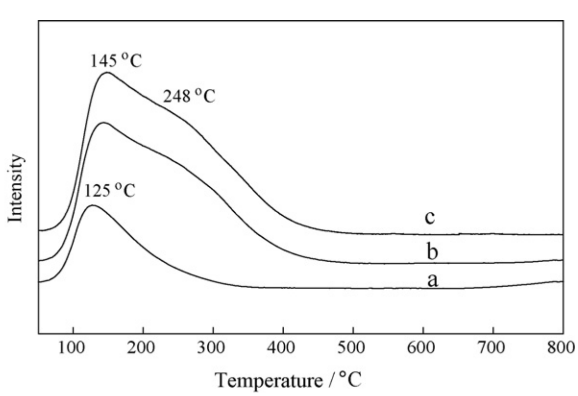

Fig. 6. CO_2-TPD profiles of catalysts: (a) Fe_2O_3–MgO/γ-Al_2O_3, (b) $Fe_2O_3/MgAl_2O_4$, and (c) $MgFe_{0.1}Al_{1.9}O_4$.

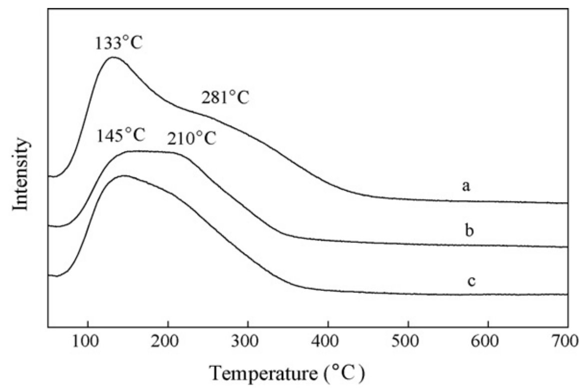

Fig. 7. NH_3-TPD profiles of catalysts: (a) Fe_2O_3–MgO/γ-Al_2O_3, (b) $Fe_2O_3/MgAl_2O_4$, and (c) $MgFe_{0.1}Al_{1.9}O_4$.

two CO_2 desorption peaks, one at ~145 °C and another in the range of 200–350 °C (Fig. 6b and c). The low-temperature peak is related to the physisorbed CO_2, while another peak is attributed to chemisorbed CO_2 on the basic center of the catalyst surface. The bigger desorption peak area for $MgFe_{0.1}Al_{1.9}O_4$ indicates that the catalyst possesses more basic sites. In contrast, Fe_2O_3–MgO/γ-Al_2O_3 sample shows only a weak CO_2-TPD peak at 125 °C.

The role of CO_2 in EBDH reaction has been concerned and discussed extensively. Liu et al. [14] reported that strong CO_2 desorption was observed in the range of 450–600 °C over La_2O_3–V_2O_5/MCM-41 catalysts. They suggested that CO_2 can react directly with the EB molecule on the catalyst surface via redox mechanism, and also react with coke (CO_2 + C = 2CO) to produce gaseous CO. Mamedov and Corberan [27] also reported that the role of CO_2 in the catalytic dehydrogenation process is removal of the deposited coke. Nevertheless, Chen et al. [28] proposed that coke deposition on the catalysts cannot be effectively suppressed by CO_2, and the role of CO_2 appears to eliminate hydrogen during EB dehydrogenation, and to keep the oxidation state of active species. In our investigation, the temperature of CO_2 desorption in TPD is lower than that of EBDH reaction, it means that the role of CO_2 in EBDH is to retain the oxidation state of active species through the remove of hydrogen in gas phase.

The acidity of the iron oxide-based catalyst greatly influences the catalytic stability. NH_3-TPD of these three catalysts was performed, and shown in Fig. 7. They all exhibit two NH_3 desorption peeks. The low-temperature peak (~140 °C) is formed by desorption of physisorbed NH_3, and the peak in the range of 180–300 °C is related to the acid sites on catalyst surface. In the sequence of $MgFe_{0.1}Al_{1.9}O_4$, $Fe_2O_3/MgAl_2O_4$ and Fe_2O_3–MgO/γ-Al_2O_3, the peaks not only shift to higher temperature, but also the strength and area increase, indicating the increase of the surface acidity. In the reaction of EBDH with CO_2, carbon deposition due to the cracking of ethylbenzene and styrene on acidic sites is one of the reasons of catalyst deactivation [14,29]. Therefore, the weak acidity of $MgFe_{0.1}Al_{1.9}O_4$ accounts for its low coke amount and excellent lifetime in the reaction.

4. Conclusions

The preparation method has great influence on the catalytic performance of iron oxide-based catalysts. The highly dispersed Fe_2O_3 can form over $Fe_2O_3/MgAl_2O_4$ prepared by the impregnation of iron nitrate solution, and in EBDH reaction, $Fe_2O_3/MgAl_2O_4$ shows very high initial activity and rapid deactivation during the reaction of EB dehydrogenation with CO_2. The α-Fe_2O_3 with large particle size in Fe_2O_3–MgO/γ-Al_2O_3 shows very low catalytic activity. BET, XRD, EDS, TPR and ^{57}Fe Mössbauer results indicated that Fe^{3+} species in $MgFe_{0.1}Al_{1.9}O_4$ catalyst is well distributed in spinel lattice, and it possesses high resistances to sintering and reduction, which are responsible for catalytic performance of the $MgFe_{0.1}Al_{1.9}O_4$ catalyst in the dehydrogenation of EB.

Acknowledgments

Financial supports by Natural Science Foundation of Liaoning Province of China (20062176), Scientific Research Foundation for Returned Scholars Ministry of Education of China, and Chinese Academy of Sciences for “100 Talents” project are gratefully acknowledged.

References

[1] E.H. Lee, Catal. Rev. 8 (1973) 285.
[2] N. Mimura, M. Saito, Catal. Lett. 58 (1999) 59.
[3] N. Mimura, M. Saito, Catal. Today 55 (2000) 173.
[4] M. Saito, H. Kimura, N. Mimura, J. Wu, K. Murata, Appl. Catal. A 239 (2003) 71.
[5] T. Badstube, H. Papp, P. Kustrowski, R. Dziembaj, Catal. Lett. 55 (1998) 169.
[6] D. Hong, V.P. Vislovskiy, Y.K. Hwang, S.H. Jhung, J. Chang, Catal. Today 131 (2008) 140.
[7] Y. Sakurai, T. Suzaki, K. Nakagawa, N. Ikenaga, H. Aota, T. Suzuki, J. Catal. 209 (2002) 16.
[8] B.S. Liu, G. Rui, R.Z. Chang, C.T. Au, Appl. Catal. A 335 (2008) 88.
[9] Y. Sakurai, T. Suzaki, N. Ikenaga, T. Suzuki, Appl. Catal. A 192 (2000) 281.
[10] N. Mimura, I. Takahara, M. Saito, Y. Sasaki, K. Murata, Catal. Lett. 78 (2002) 125.
[11] D.R. Burri, K.M. Choi, S.D. Han, N. Jiang, A. Burri, S.E. Park, Catal. Today 131 (2008) 173.
[12] M. Sugino, H. Shimada, T. Turuda, H. Miura, N. Ikenaga, T. Suzuki, Appl. Catal. A 121 (1995) 125.
[13] T. Badstube, H. Papp, R. Dziembaj, P. Kustrowski, Appl. Catal. A 204 (2000) 153.
[14] B.S. Liu, R.Z. Chang, L. Jiang, W. Liu, C.T. Au, J. Phys. Chem. C 112 (2008) 15490.
[15] B.M. Reddy, S.Ch. Lee, D.S. Han, S.E. Park, Appl. Catal. B 87 (2009) 230.
[16] P.Y. Lee, H. Suematsu, T. Yano, K. Yatsui, J. Nanopart. Res. 8 (2006) 911.
[17] A. Banerjee, S. Das, S. Misra, S. Mukhopadhyay, Ceram. Int. 35 (2009) 381.
[18] S. Angappan, L. John Berchmans, C.O. Augustin, Mater. Lett. 58 (2004) 2283.
[19] X. Ge, M.S. Li, J.Y. Shen, J. Solid State Chem. 161 (2001) 38.
[20] Y. Ohishi, T. Kawabata, T. Shishido, K. Takaki, Q.H. Zhang, Y. Wang, K. Nomura, K. Takehira, Appl. Catal. A 288 (2005) 220.
[21] M. Liu, H.B. Li, L. Xiao, W.X. Yu, Y. Lu, Z.D. Zhao, J. Magn. Magn. Mater. 294 (2005) 294.
[22] S. Herreyre, P. Gadelle, P. Moral, J.M. Miliet, J. Phys. Chem. Solids 58 (1997) 1539.
[23] M. Tu, J.Y. Shen, Y. Chen, J. Solid State Chem. 128 (1997) 73.
[24] P.S. Kumbhar, J. Sanchez-Valente, J.M.M. Millet, F. Figueras, J. Catal. 191 (2000) 467.
[25] V. Carles, A. Rousste, Solid State Ionics 83 (1996) 309.
[26] P. Coquay, E.D. Garve, R.E. Vandenberghe, C. Dauwe, E. Flahaut, C.H. Laurent, A. Peigney, A. Rousset, Acta Mater. 48 (2000) 3015.
[27] E.A. Mamedov, V.C. Corberan, Appl. Catal. A 127 (1995) 1.
[28] Sh.W. Chen, Zh.F. Qin, X.F. Xu, J.G. Wang, Appl. Catal. A 302 (2006) 185.
[29] Y. Ohishi, T. Kawabata, T. Shishido, K. Takaki, Q.H. Zhang, Y. Wang, K. Takehira, J. Mol. Catal. A 230 (2005) 49.